Comprehensive knockout analysis of the Rab family GTPases in epithelial cells

TOOLS

Comprehensive knockout analysis of the Rab family GTPases in epithelial cells

Yuta Homma, Riko Kinoshita, Yoshihiko Kuchitsu, Paulina S. Wawro, Soujiro Marubashi, Mai E. Oguchi, Morié Ishida, Naonobu Fujita, and Mitsunori Fukuda

The Rab family of small GTPases comprises the largest number of proteins (∼60 in mammals) among the regulators of intracellular membrane trafficking, but the precise function of many Rabs and the functional redundancy and diversity of Rabs remain largely unknown. Here, we generated a comprehensive collection of knockout (KO) MDCK cells for the entire Rab family. We knocked out closely related paralogs simultaneously (Rab subfamily knockout) to circumvent functional compensation and found that Rab1A/B and Rab5A/B/C are critical for cell survival and/or growth. In addition, we demonstrated that Rab6-KO cells lack the basement membrane, likely because of the inability to secrete extracellular matrix components. Further analysis revealed the general requirement of Rab6 for secretion of soluble cargos. Transport of transmembrane cargos to the plasma membrane was also significantly delayed in Rab6-KO cells, but the phenotype was relatively mild. Our Rab-KO collection, which shares the same background, would be a valuable resource for analyzing a variety of membrane trafficking events.

Introduction

How intracellular membrane compartments acquire their identity and communicate with each other is a fundamental question in cell biology. One of the key players in these processes is the Rab family of small GTPases that comprises ∼60 genes in mammals. Each Rab protein localizes to specific intracellular membrane compartments in their GTP-bound form (active form) and recruits effector proteins that aid various steps in membrane trafficking, including budding, transport, tethering, docking, and fusion of vesicles or organelles (Fukuda, 2008; Stenmark, 2009; Hutagalung and Novick, 2011; Pfeffer, 2013). For example, Rab5 localizes on early endosomes and interacts with early endosome antigen 1 (EEA1) for endosome tethering and close approximation (Simonsen et al., 1998; Murray et al., 2016), while Rab27 recruits the Slac2-a/myosin-Va complex on melanosomes, thereby enabling actin-dependent peripheral transport (Fukuda et al., 2002; Wu et al., 2002). Although a small number of Rabs have been intensively studied, so far the majority of them have been assigned few or no effectors and detailed functions, and thus we are still far from complete functional annotation of all of the Rabs in mammals.

The functions of the Ras-superfamily small GTPases can be investigated by overexpressing their constitutively negative mutants (Feig, 1999). The constitutively negative form of Ras (Ras(T17N)) is thought to sequester guanine nucleotide exchange factors (GEFs) of Ras by forming a nonfunctional complex and thereby prevent activation of endogenous Ras. Although similar constitutively negative Rab mutants are widely used to investigate the function of Rabs in membrane trafficking, none of them has been demonstrated to act by the same GEF-trap mechanism. Moreover, the situation becomes complicated when one GEF is responsible for activating multiple Rabs (Delprato et al., 2004; Homma and Fukuda, 2016), because the dominant-negative effect of a constitutively negative Rab mutant on the corresponding GEF should nonspecifically extend to the other substrate Rabs. Knockdown with siRNA, a well-established and widely used method for depleting a specific gene of interest, also has the disadvantage that elimination of the target protein is often incomplete, which makes the interpretation of results difficult. In fact, the roles of Rab8 that have been revealed in knockout (KO) mice are different from those previously suggested by mutant overexpression or siRNA knockdown experiments (Nachury et al., 2007; Sato et al., 2007, 2014). Thus, more solid information about loss-of-function phenotypes of Rabs is needed to understand how all of the Rab family proteins orchestrate intracellular membrane trafficking.

Laboratory of Membrane Trafficking Mechanisms, Department of Integrative Life Sciences, Graduate School of Life Sciences, Tohoku University, Miyagi, Japan.

Correspondence to Mitsunori Fukuda: mitsunori.fukuda.c1@tohoku.ac.jp;   P.S. Wawro's present address is Dept. of Biochemistry, Stanford University School of Medicine, Stanford, CA;   M. Ishida's present address is Cell Biology and Neurobiology Branch, Eunice Kennedy Shriver National Institute of Child Health and Human Development, National Institutes of Health, Bethesda, MD.

Cas9-mediated genome editing technology has made it quite easy to disrupt specific genes in a variety of animals and cultured cells (Cong et al., 2013; Mali et al., 2013). Taking advantage of this technology, we established a complete collection of KO MDCK cells (a well-known epithelial cell line) for all of the mammalian Rab genes. Through immunofluorescence analyses of several organelles and 3D-cultured cysts, we were able to validate roles of some Rabs, but KO of other Rabs did not recapitulate their previously reported phenotypes. We especially focused on Rab6, whose deficiency resulted in lack of the basement membrane, likely due to inability to secrete ECM components. Further analysis revealed that Rab6 is generally required for secretion of soluble cargos, whereas inhibition of transmembrane cargos in Rab6-KO cells was relatively mild. Our collection of Rab-KO cells provides a powerful platform for comprehensive comparison of Rab-KO phenotypes, because the cells share the same background (i.e., were obtained from the same parental cell line), making the collection a unique and valuable resource for application in many fields involving membrane trafficking.

Results

Establishing a comprehensive collection of Rab-KO MDCK cells

To investigate the role of Rab family small GTPases, we sought to generate a collection of KO cell lines for all of the mammalian Rabs. We chose MDCK cells because of their easy handling and our interest in polarized membrane trafficking. To circumvent functional compensation by closely related paralogs (e.g., Rab1A/B), we tried to knock out these paralogs simultaneously (hereafter "Rab1" represents both Rab1A and Rab1B, and so forth). Such "Rab-subfamily KO" is simply referred to as "Rab-KO" hereafter, and the combinations of Rab KOs and their target sequences are listed in Tables 1 and S1. By introducing indels into the coding sequence of Rab genes using a previously reported Cas9/single guide RNA–expressing vector (Ran et al., 2013), we succeeded in generating all Rab-KO cell lines except Rab1-KO and Rab5-KO cell lines. Some of the Rab-KO clones (i.e., Rab4A/B, 10, 11B, and 22A) have nonframeshift mutations (Tables 1 and S1), but all of these mutations occur in the highly conserved phosphate/magnesium/guanine base-binding motifs or switch regions (as indicated in Extended Fig. S1 in the BioStudies database, https://www.ebi.ac.uk/biostudies; accession no. S-BSST239), and the drastic reduction of the mutant Rab protein levels of all these clones were observed by immunoblotting (Fig. S1). Actually, a FLAG-tagged Rab10(ΔI) mutant was hardly detected even when it was overexpressed in MDCK cells (Fig. S2 A), indicating that this mutation makes Rab10 quite unstable. Although the expression levels of Rab4A(ΔR) and Rab22A(ΔT) mutants were similar (or slightly decreased) versus those of their wild-type Rabs (Fig. S2, A and B), these mutant proteins were almost cytosolic in contrast to the normal endosomal localization of Rab4A and Rab22A (Fig. S2 C), suggesting that they are nonfunctional even if they are faintly expressed in KO cells. These cells, together with expression plasmids of all of the mammalian Rabs with EGFP-tag (for rescue experiments), are available from RIKEN Bioresource Center in Japan (http://en.brc.riken.jp/index.shtml).

Rab1 and Rab5 are essential for cell survival and/or growth

We failed to obtain Rab1A/B double-KO cells even though Rab1A-KO and Rab1B-KO cells were viable, raising the possibility that Rab1 is essential for survival of MDCK cells. To determine whether simultaneous loss of Rab1A/B is lethal, we performed a knockdown experiment using siRNAs, but neither control siRNA (siControl) nor two independent siRNAs against Rab1A (siRab1A) induced cell death in parental cells. By contrast, Rab1B-KO cells that had been transfected with siRab1A, but not with siControl, gradually died off, and as a result the cell numbers were much lower than the number of parental cells 3 d after transfection (Fig. 1, A and B). This effect was rescued by expressing EGFP-Rab1B, indicating that Rab1A and B have a redundant role for cell survival, consistent with a previous report demonstrating that KO of Rab1A/B is synthetic lethal in a haploid human cell line (Blomen et al., 2015).

We also failed to obtain Rab5A/B/C triple-KO cells, although Rab5A-KO, Rab5B-KO, Rab5A/B-KO, and Rab5C-KO cells were viable. Unlike the case of Rab1, knockdown of Rab5C in Rab5A/B-KO cells did not lead to an apparent cell death phenotype, but cell growth seemed to be retarded, and cell morphology was distorted (Fig. 1 C). To further assess the effect of Rab5 deficiency on cell growth, we used a mixture of Rab5A/B-KO cells, about half of which stably expressed Myc-Rab5A. If loss of Rab5A/B/C inhibited cell growth and it could be rescued by exogenous Myc-Rab5A, long-term knockdown of Rab5C would decrease the proportion of Myc-Rab5A(–) cells in this mixture. In fact, during the sequential passage and siRab5C transfection, the proportion of Myc-Rab5A(–) cells did gradually decline, reaching <5% after the third transfection, whereas siControl had no effect (Fig. 1 D). These results indicated that both Rab1 and Rab5 are critical for the survival and/or growth of MDCK cells, thereby explaining why we were unable to generate their KO cells.

Effect of Rab-KO on organelle morphology

The Rab-KO cells established above were first subjected to immunofluorescence analysis for several intracellular organelles, including the ER (reticulon 4), the Golgi (polypeptide N-acetylgalactosaminyltransferase 2 [GalNT2]), early endosomes (EEA1), recycling endosomes (transferrin receptor [TfR]), and lysosomes (lysosomal associated membrane protein 2 [LAMP2]). Only the images of Rab-KO cells with marked alterations in these organelles are shown in Fig. S3; all other images can be downloaded from BioStudies (Extended Fig. S2). Consistent with a previous report (Aizawa and Fukuda, 2015), the Golgi in Rab2-KO cells was fragmented and dispersed throughout the cell, and this phenotype was rescued by expressing either Myc-Rab2A or Myc-Rab2B (Fig. 2 A). In addition, the Golgi in Rab6-KO cells was often swollen, and GalNT2 staining was greatly diminished in a portion (~20%) of the cells, and these phenotypes were rescued by expressing EGFP-Rab6A (Fig. 2 B).

Another remarkable phenotype is enlarged lysosomes in Rab7A-KO cells, which was most likely caused by lysosomal dysfunction (Fig. 2 C; Kuchitsu et al., 2018). In addition, consistent with previous reports (Rojas et al., 2008; Modica

Homma et al.
Comprehensive Rab knockout in epithelial cells

Journal of Cell Biology 2036
https://doi.org/10.1083/jcb.201810134

Table 1. Rab KOs and their indel information

KO cell line	Rab name[a]	Mutation	KO check by immunoblotting
Rab1A	Rab1A	−16 nt	Yes
Rab1B	Rab1B	+1 nt/−86 nt	Yes
Rab2	Rab2A	−4 nt/+1 nt	Yes
	Rab2B	+1 nt	Yes
Rab3	Rab3A	−113 nt	Yes
	Rab3B	+1 nt	
	Rab3C	−8 nt	
	Rab3D	+2 nt	Yes
Rab4	Rab4A	+1 nt/−3 nt	Yes
	Rab4B	+1 nt/−12 nt	Yes
Rab5AB	Rab5A	+1 nt	Yes
	Rab5B	+1 nt/−5 nt	Yes
Rab5C	Rab5C	+1 nt	Yes
Rab6	Rab6A	+1 nt/−1 nt	Yes
	Rab6B	+1 nt/+2 nt	Yes
Rab7A	Rab7A	+1 nt/+1 nt/−2 nt	Yes
Rab7B	Rab7B (42)	+1 nt	
Rab8	Rab8A	−2 nt	Yes
	Rab8B	+2 nt	Yes
Rab9	Rab9A	+2 nt	
	Rab9B	+1 nt	
Rab10	Rab10	−2 nt/−3 nt	Yes
Rab11	Rab11A	+1 nt/−5 nt	Yes
	Rab11B	+9 nt/−9 nt	Yes
Rab12	Rab12	+1 nt	
Rab13	Rab13	+1 nt	Yes
Rab14	Rab14	+1 nt	Yes
Rab15	Rab15	+1 nt/+4 nt	Yes
Rab17	Rab17	+1 nt/+1 nt	
Rab18	Rab18	+1 nt	Yes
Rab19	Rab19	+1 nt	Yes
Rab20	Rab20	+1 nt/−1 nt	Yes
Rab21	Rab21	+1 nt/−4 nt	Yes
Rab22	Rab22A	+1 nt/−3 nt	Yes
	Rab31 (22B)	+1 nt	
Rab23	Rab23	+1 nt/+1 nt	
Rab24	Rab24	+1 nt	Yes
Rab25	Rab25	+1 nt	
Rab26	Rab26	+1 nt	
Rab27	Rab27A	+1 nt	Yes
	Rab27B	+1 nt/+2 nt	
Rab28	Rab28	+1 nt	
Rab29	Rab29 (7L1)	+1 nt/−1 nt	

Table 1. Rab KOs and their indel information (Continued)

KO cell line	Rab name[a]	Mutation	KO check by immunoblotting
Rab30	Rab30	+1 nt	Yes
Rab32/38	Rab32	+2 nt/+2 nt	Yes
	Rab38	+1 nt	
Rab33	Rab33A	+1 nt/+1 nt	
	Rab33B	+1 nt	Yes
Rab34	Rab34	+2 nt	Yes
Rab35	Rab35	+1 nt	Yes
Rab36	Rab36	+1 nt	
Rab37	Rab37	+1 nt	
Rab39	Rab39A	+251 nt	Yes
	Rab39B	+1 nt	Yes
Rab40	Rab40B	+1 nt	
	Rab40C	−1 nt	
Rab42	Rab42 (43)	−7 nt	
Rab43	Rab43 (41)	−1 nt	

[a]The nomenclature of Rabs in this study is according to that of the National Center for Biotechnology Information database.

et al., 2017), premature cathepsin B, which is normally sorted to lysosomes with the help of mannose 6-phosphate receptor (M6PR), leaked into the medium of the Rab7A-KO cells, but not into the medium of the parental cells (Fig. 2 D). On the other hand, although Rab9 has also been reported to regulate M6PR recycling (Riederer et al., 1994), Rab9-KO cells showed no visible defects in lysosomes or cathepsin B secretion defects in contrast to the Rab7A-KO cells (Fig. 2, C and D). Because of the relatively high sequence similarity between Rab7A and Rab9, we hypothesized that Rab7A compensates for the function of Rab9 in Rab9-KO cells and then proceeded to investigate the potential genetic interaction between Rab7A and Rab9. Indeed, we found that Rab7A/9A/9B-KO cells exhibited even larger lysosomes and greater cathepsin B secretion than Rab7A-KO cells did (Fig. 2, C and D). Moreover, decreased EEA1 signals were observed in Rab5A/B-KO cells (Fig. S3), consistent with the fact that EEA1 functions as a Rab5 effector (Simonsen et al., 1998). Thus, the results obtained in our Rab-KO cells clearly confirmed previously reported functions of several Rabs in organelle homeostasis in a more reliable manner.

Effect of Rab-KO on epithelial morphogenesis
Next, we investigated the roles of Rab GTPases in epithelial morphogenesis. When MDCK cells are plated and reach confluence on a flat substrate, they tightly contact each other through cellular junctions to form an epithelial monolayer. In all Rab-KO cells, we were able to observe tight junction network by immunostaining of zonula occludens 1 (data not shown), indicating that none of the Rab subfamilies is essential for monolayer formation.
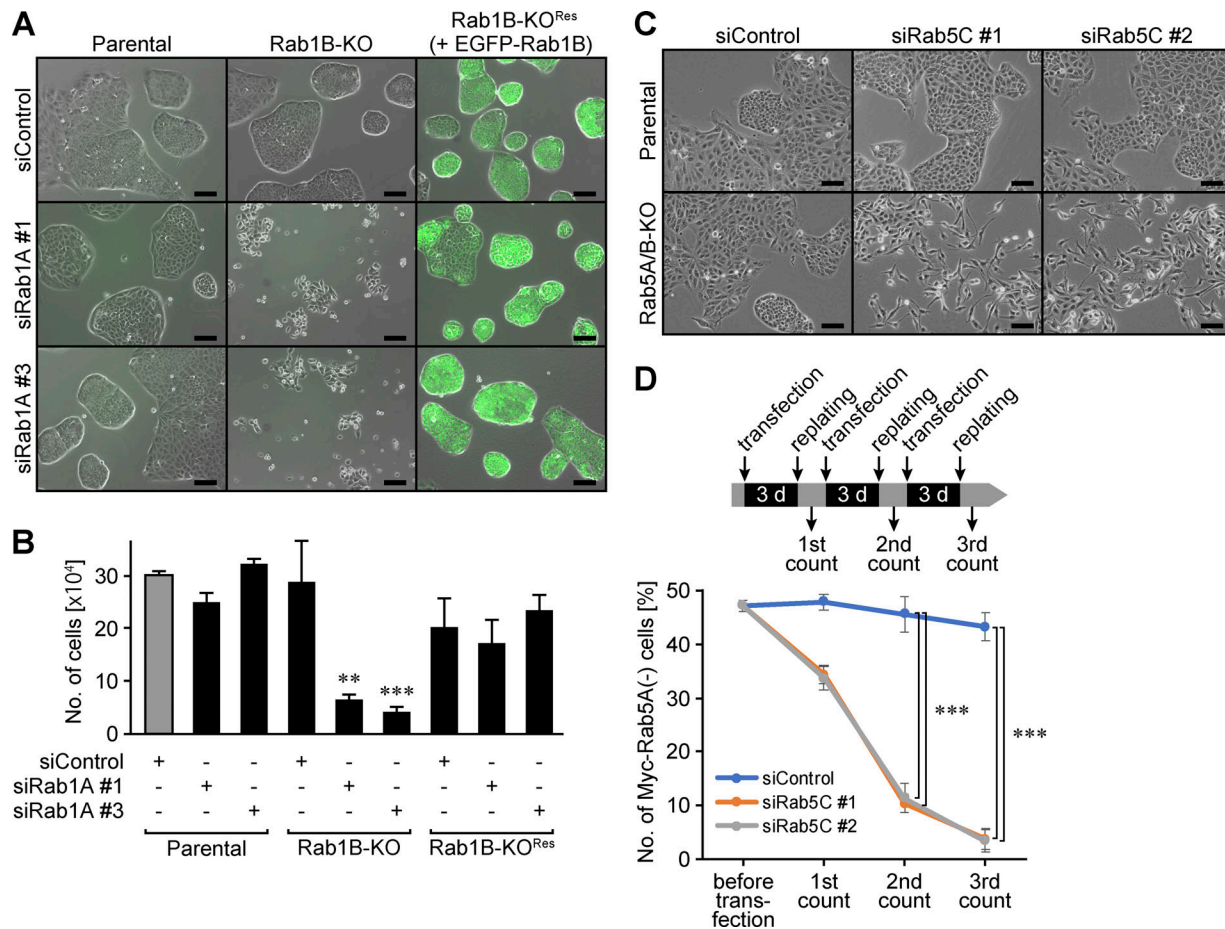
Figure 1.   Rab1 and Rab5 are essential for survival and/or growth of MDCK cells. (A and B) Rab1A knockdown in Rab1B-KO cells. Parental, Rab1B-KO, and its rescue (+EGFP-Rab1B) cells were plated at 1×10^4 cells/well and transfected with siControl or siRab1A (#1 and #3). After 72-h culture, cell numbers were counted (B). **, $P < 0.01$; ***, $P < 0.001$ ($n = 3$; Dunnett's test). The phase-contrast images with EGFP fluorescence were taken before trypsinization for the cell count (A). Scale bars, 100 µm. **(C and D)** Rab5C knockdown in Rab5A/B-KO cells. Parental and Rab5A/B-KO cells were transfected with siControl or siRab5C (#1 and #2) and cultured for 72 h (C). Scale bars, 100 µm. A mixture of Rab5A/B-KO cells, about half of which express Myc-Rab5A, were transfected with siControl or siRab5C (#1 and #2). The cells were cultured for 3 d, replated, and again transfected with the respective siRNAs. This cycle was repeated three times, and the proportion of Myc-Rab5A(−) cells was calculated after each replating (D). ***, $P < 0.001$ ($n = 3$; Tukey's test). See also Figs. S1 and S2.

MDCK cells are also known to develop a spherical epithelial architecture called a cyst when embedded in an ECM gel such as collagen or Matrigel. To determine whether Rab-KO affects epithelial polarity formation, we stained apical and basolateral membranes with anti-ezrin and anti–E-cadherin antibodies, respectively. Consistent with previous reports (Bryant et al., 2010; Mrozowska and Fukuda, 2016), we observed that the Rab11-KO cysts had multiple small lumens and that this phenotype was completely rescued by expressing EGFP-Rab11A (Figs. 4 A and S4). KO of Rab11A alone did not induce this phenotype (Fig. S5 A), indicating that Rab11A and B redundantly function in proper cyst formation. Although several Rabs, such as Rab3, Rab8, and Rab27, have also been shown to be involved in single lumen formation (Bryant et al., 2010; Gálvez-Santisteban et al., 2012; Vogel et al., 2015; Mrozowska and Fukuda, 2016), no Rab-KO cells except Rab11-KO cells exhibited the strong multilumen phenotype, at least under our experimental conditions (Fig. S4 and Extended Fig. S3 in BioStudies).

We next focused on the basement membrane, the layer of ECM formed beneath the basal face of an epithelial sheet. The cysts of parental cells were clearly surrounded by immunofluorescent signals of laminin, one of the major components of the basement membrane (Fig. 3, parental). However, we found that laminin staining was markedly diminished only in Rab6-KO cysts and that expression of EGFP-Rab6A rescued this phenotype (Fig. 3 and Fig. 4, B and C). Although Rab6B is predominantly expressed in brain (Opdam et al., 2000), loss of Rab6A alone is insufficient to result in this defect (Fig. 4 B), indicating that Rab6B compensates for Rab6A function even in nonneuronal cells.

We then assessed basement membrane formation by Rab6-KO cells in more quantitative ways. Parental and Rab6-KO cells were grown on culture dishes for 2 d. After, they were removed by treatment with 20 mM ammonium hydroxide and the remaining ECM on the dish was dissolved in SDS sample buffer and analyzed by immunoblotting. Consistent with the results of immunostaining, laminin β1/γ1 and γ2 chains were detected in the ECM of parental cells, but not of Rab6-KO cells (two
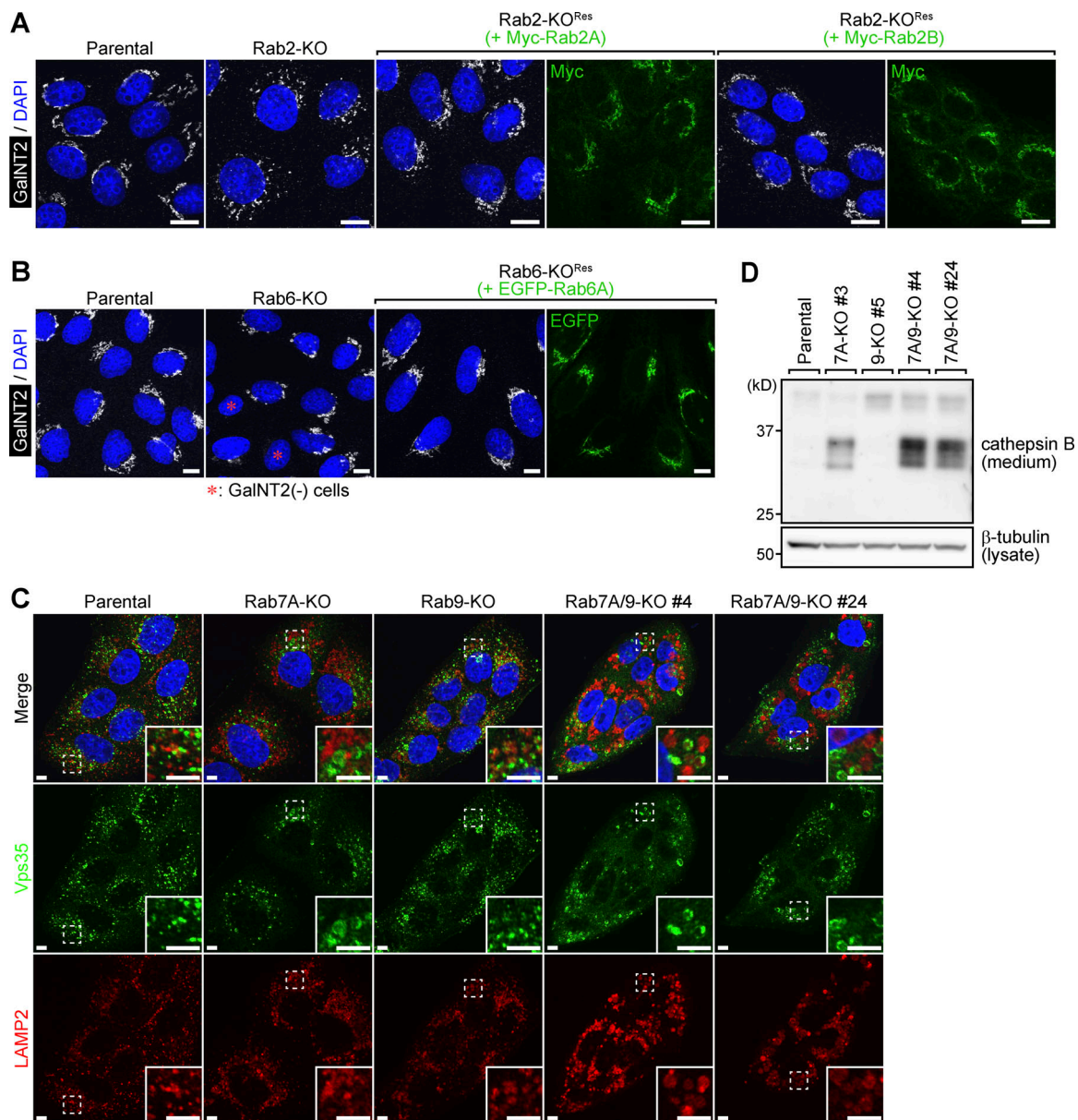
Figure 2. **Effect of Rab2-, Rab6-, and Rab7A-KO on organelle morphology. (A)** Immunostaining of the Golgi in Rab2-KO cells. Parental, Rab2-KO, and its rescue (+Myc-Rab2A or Myc-Rab2B) cells were immunostained with anti-GalNT2 (white) and anti-Myc (green) antibodies (DAPI in blue). Scale bars, 10 μm. **(B)** Immunostaining of the Golgi in Rab6-KO cells. Parental, Rab6-KO (clone #7), and its rescue (+EGFP-Rab6A) cells were immunostained with an anti-GalNT2 (white) antibody (DAPI in blue). The asterisks indicate the Rab6-KO cells with no GalNT2 staining. **(C)** Immunostaining of lysosomes in Rab7A-KO, Rab9-KO, and Rab7A/9-KO cells. Parental, Rab7A-KO, Rab9-KO, and Rab7A/9-KO cells were immunostained with anti-Vps35 (green) and anti-LAMP2 (red) antibodies (DAPI in blue). The insets show the magnified views of the boxed areas. Scale bars, 5 μm. **(D)** Immunoblot analysis of secreted cathepsin B in Rab7A-KO, Rab9-KO, and Rab7A/9-KO cells. Conditioned media from parental, Rab7A-KO, Rab9-KO, and Rab7A/9-KO cells were analyzed by immunoblotting with an anti-cathepsin B antibody. See also Fig. S3.

independent clones, #7 and #39), and the phenotypes of both clones were completely rescued by expressing EGFP-Rab6A (Fig. 4 D, ECM). In addition, silver staining of the ECM samples revealed the absence not only of laminin but of most other high-molecular-weight bands, which probably corresponded to such ECM proteins as fibronectin, collagens, and proteoglycans, in the Rab6-KO cells (Fig. 4 E). Again, expression of EGFP-Rab6A in Rab6-KO cells clearly restored the high-molecular-weight bands in the ECM fraction (Fig. 4 E). Taken together, these results suggest that Rab6 is essential for ECM formation.

Rab6 is required for soluble and transmembrane cargo secretion

Since Rab6 is known to regulate transport of anterograde cargos such as vesicular stomatitis virus glycoprotein (VSVG) to the plasma membrane (Grigoriev et al., 2007; Miserey-Lenkei et al., 2010; Storrie et al., 2012; Johns et al., 2014), and the levels of ECM protein expression appeared to be normal even in Rab6-KO cells (Fig. 4 D, Lysate), we hypothesized that the secretion of ECM components is inhibited in Rab6-KO cells. To evaluate protein secretion, after culturing parental and Rab6-KO cells in
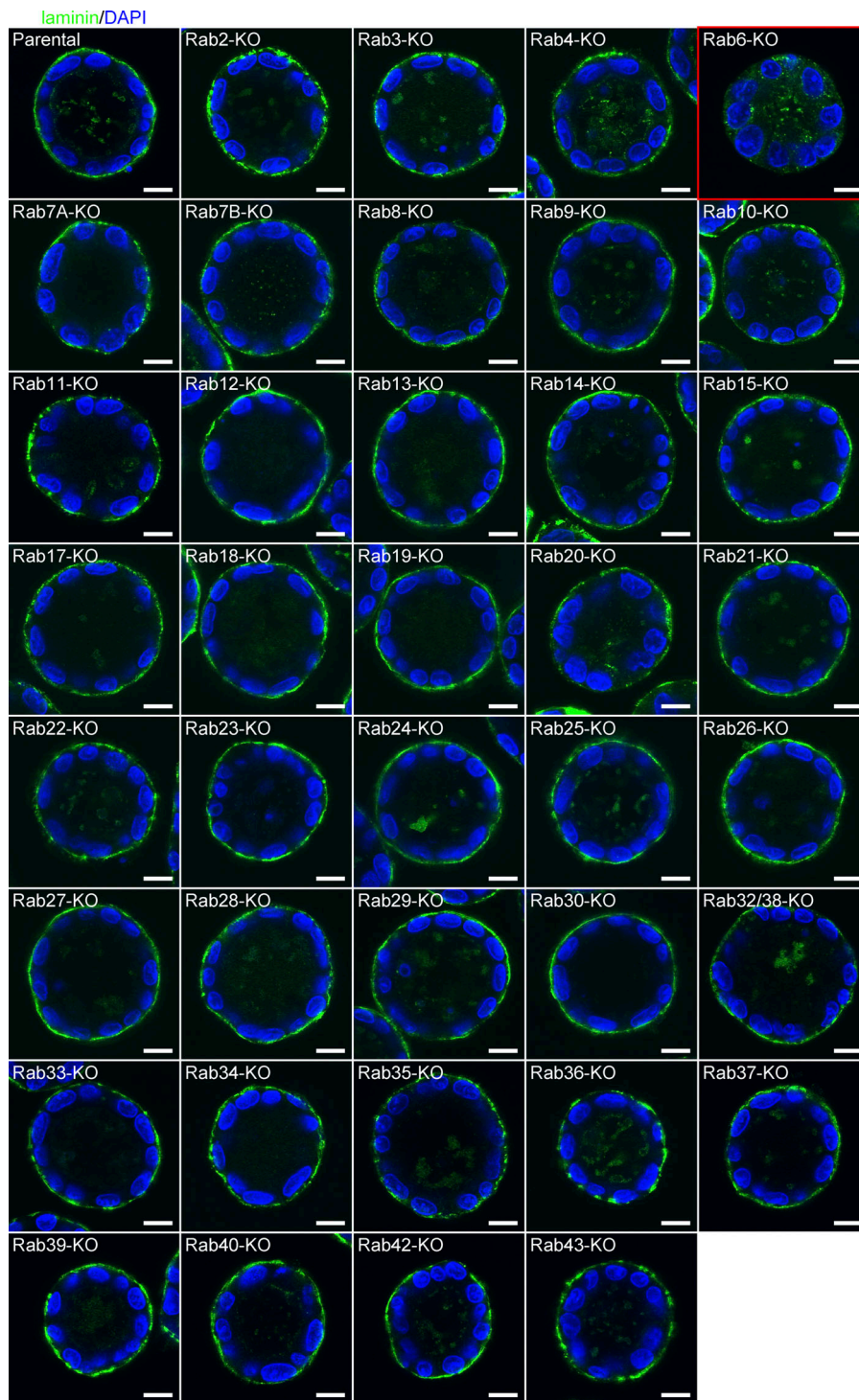
Figure 3. **Immunostaining of laminin in Rab-KO cysts.** Rab-KO cysts grown in collagen gel for 7 d were fixed with TCA and immunostained with an anti-laminin antibody. Scale bars, 10 μm. The red box indicates Rab6-KO cysts that lack laminin staining.

serum-free medium for 20 h, we analyzed the total secreted proteins in the medium by immunoblotting. As expected, hardly any laminins were detected in the conditioned medium from Rab6-KO cells (Fig. 4 D, Medium), suggesting that the defect in ECM formation in Rab6-KO cells is caused by inability to secrete ECM components into the extracellular region.

The next question is the specificity of the secretory defect observed in Rab6-KO cells, that is, whether Rab6 is required for secretion of ECM components alone or for secretion of a wider range of secretory proteins. To answer this question, we labeled the total secreted proteins from parental cells and Rab6-KO cells with isobaric tags and analyzed them by quantitative mass spectrometry (isobaric tag for relative and absolute quantitation [iTRAQ]). We identified 838 proteins, and the full list sorted by confidence is shown in Table S2. Of the top 100 proteins, 26 were secretory proteins harboring a signal sequence, and the others included unconventional secretory proteins, cytosolic proteins, ER or lysosomal resident proteins, and transmembrane
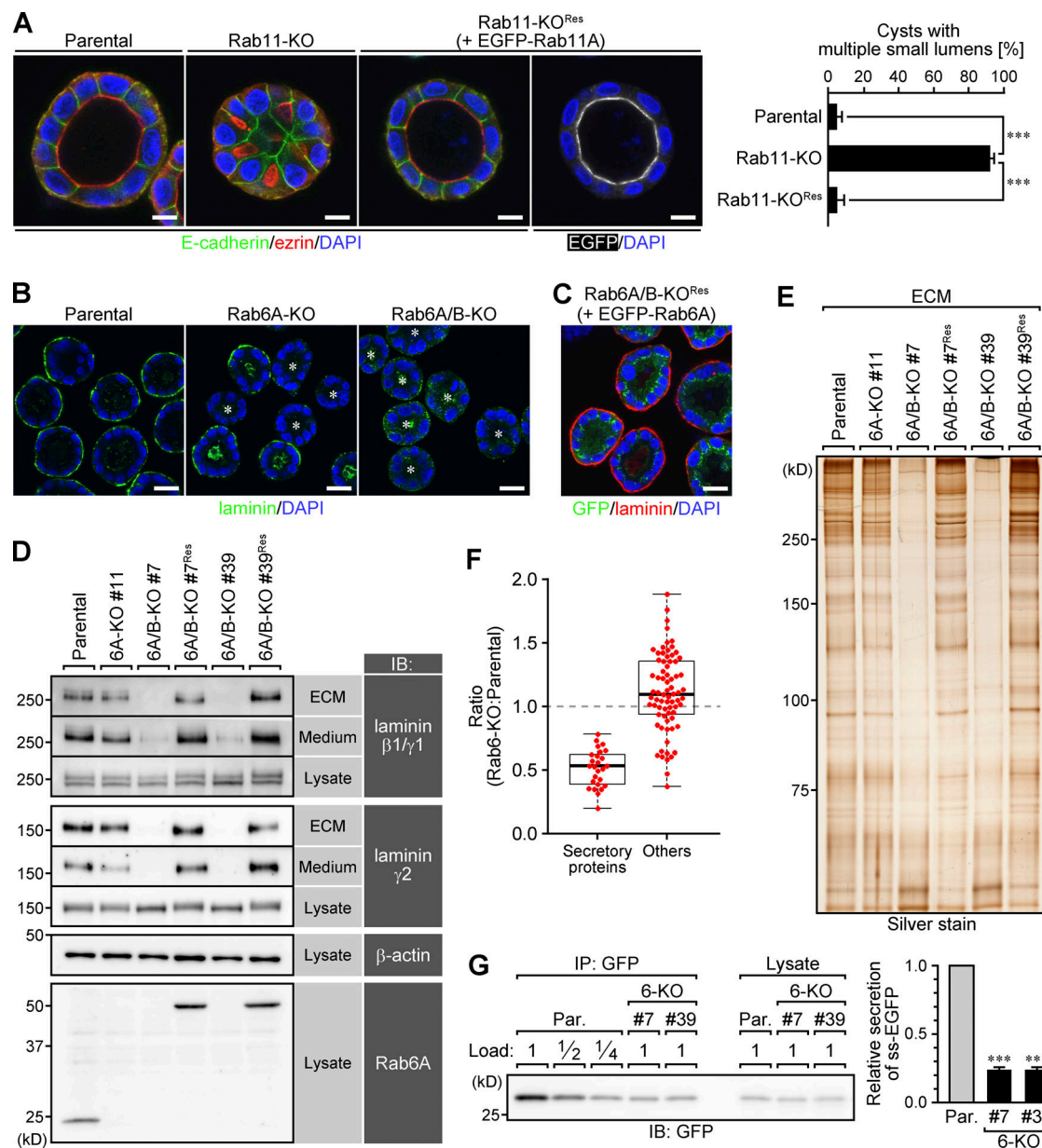
Figure 4. **Rab6 and Rab11 are required for normal epithelial morphogenesis. (A)** Immunostaining of ezrin and E-cadherin in Rab11-KO cysts. Parental, Rab11-KO, and its rescue (+EGFP-Rab11A) cells were cultured in collagen gel for 7 d. The cells were fixed with TCA and immunostained with anti-ezrin (red) and anti–E-cadherin (green) antibodies. Scale bars, 10 µm. The graph shows the percentages of cysts with multiple small lumens (50 cells per experiment). Data are means and SEM. ***, P < 0.001 (n = 3; Dunnett's test). **(B and C)** Immunostaining of laminin in Rab6-KO and its rescue cysts. Parental, Rab6A-KO, Rab6A/B-KO (clone #7), and its rescue (+EGFP-Rab6A) cells were cultured in collagen gel for 7 d. The cells were then fixed with TCA and immunostained with an anti-laminin antibody (green in B and red in C). The asterisks indicate the cysts with no laminin staining at the basal surface. Scale bars, 20 µm. **(D)** Immunoblot (IB) analysis of laminin in ECM and conditioned medium from Rab6-KO cells. ECM, total secreted proteins (Medium), and lysates from parental, Rab6A-KO, Rab6A/B-KO (clones #7 and #39), and their rescue (+EGFP-Rab6A) cells were analyzed by immunoblotting. **(E)** Silver staining of ECM samples shown in D. **(F)** Quantitative mass spectrometry for total secreted proteins from parental and Rab6-KO cells. Total secreted proteins from parental and Rab6-KO (clone #7) cells were subjected to iTRAQ-based quantitative mass spectrometry. The proteins identified with high confidence (top 100) were classified into secretory proteins and the others, and then Rab6-KO/parental ratios of their abundance were plotted as red dots. The center lines of the box plot represent the medians of each group of data. **(G)** Secretion of ss-EGFP in parental and Rab6-KO cells. Parental and Rab6-KO cells that stably express ss-EGFP were allowed to secrete ss-EGFP into the medium for 6 h, and then the secreted ss-EGFP was immunoprecipitated (IP) with an anti-GFP nanobody. The graph represents quantification of the band intensities normalized to that of parental cells. Data are means and SEM. ***, P < 0.001 (n = 3; Dunnett's test). See also Figs. S4 and S5.

proteins. We compared the Rab6-KO/parental ratios of abundance of the reporter tag in each protein and found that the ratios of all 26 secretory proteins were <1.0 (median 0.53), while those of the other proteins were ~1.0 (median 1.10; Fig. 4 F). The

results of the analysis of total secreted proteins by silver staining and immunoblotting are shown in Fig. S5 (B and C). To further corroborate the global inhibition of the conventional secretory pathway in Rab6-KO cells, we used signal sequence–fused EGFP

(ss-EGFP) as a model cargo without any specific sorting signal. Indeed, secretion of ss-EGFP from Rab6-KO cells for 6 h was also decreased to ~25% of that in parental cells (Fig. 4 G), and the amount of secreted ss-EGFP was not increased even after 24-h culture (not depicted). These findings indicate that loss of Rab6 inhibits not only secretion of ECM components but secretion of other secretory proteins as well.

If Rab6 is required for the conventional secretory pathway, delivery of transmembrane proteins to the cell surface should also be inhibited in the absence of Rab6. To assess the trafficking efficiency of transmembrane proteins, we fused a conditional aggregation domain (FM4; Rivera et al., 2000) to ss-EGFP, followed by a transmembrane domain of LDL receptor (ss-EGFP-FM4-TM; Fig. 5 A). This construct enabled a synchronized trafficking assay, in which trafficking is triggered by adding a disaggregation drug (D/D solubilizer). At 120 min after addition of the drug, the model cargo was significantly delivered to the cell surface even in Rab6-KO cells; however, its delivery seemed less efficient than in parental cells (Fig. 5 A). A surface biotinylation assay revealed that surface expression of the model cargo in Rab6-KO cells was about half of that in parental cells (Fig. 5 B). We also investigated the expression levels of several endogenous plasma membrane proteins (podocalyxin/gp135, β1-integrin, and TfR) of parental and Rab6-KO cells and found that their expression levels appeared not to be different in the steady state (Fig. 5 C). We therefore concluded that secretion of soluble cargos is severely inhibited in Rab6-KO cells, whereas secretion of transmembrane cargos is mildly impaired.

Rab6 has been reported to be involved in several steps in the secretory pathway: intra-Golgi transport, exit from the Golgi, and transport and tethering of the post-Golgi vesicles to the plasma membrane (Martinez et al., 1994; Grigoriev et al., 2007; Miserey-Lenkei et al., 2010). To identify the impaired steps in Rab6-KO cells, the fate of ss-EGFP in Rab6-KO cells was chased by treating with a translation inhibitor, cycloheximide (CHX). The results showed that even in Rab6-KO cells, the intracellular ss-EGFP signal almost disappeared within 6 h (Fig. 6 A), even though ss-EGFP secretion was strongly inhibited (Fig. 4 G). This finding was confirmed by immunoblotting of cell lysates after CHX treatment (Fig. 6 B). In addition, synchronized traffic of ss-EGFP-FM4 revealed normal passage of the cargo through the Golgi (Fig. S6 A). ss-EGFP-FM4, which initially localized at the ER, was transported to the Golgi and colocalized with GM130 (*cis*-Golgi marker) 30 min after D/D solubilizer treatment, and then disappeared at 120 min. These results indicate that secretory traffic from the ER to the Golgi in Rab6-KO cells is normal, and thus Rab6 is likely to be required for the steps after exiting from the Golgi.

If the unsecreted ss-EGFP in Rab6-KO cells also disappeared, where did it go? Assuming that unsecreted cargos in Rab6-KO cells are degraded in lysosomes, we attempted to block degradation of ss-EGFP by using a lysosomal inhibitor, bafilomycin A1 (BafA1). Indeed, BafA1 significantly increased the amount of intracellular ss-EGFP in Rab6-KO cells, but had no effect on parental cells (Fig. 6 B). We also found that immunostaining for ss-EGFP with an anti-GFP antibody detected lysosomally targeted ss-EGFP in Rab6-KO cells, but not in parental cells, and that the signal was dramatically increased by treatment with BafA1 (Fig. 6, C and D). Endogenous laminin also accumulated in lysosomes when Rab6-KO cells, but not parental cells, were treated with the lysosomal enzyme inhibitors E64d and pepstatin A (Fig. S6 B). These results taken together indicate that secretory cargos can exit the Golgi but cannot reach the plasma membrane in Rab6-KO cells, and that unsecreted cargos are mistargeted to lysosomes for degradation.

Discussion

The comprehensive collection of Rab-KO cells with consideration of functional redundancy

In this study, we established a KO cell collection for all Rab family small GTPases that are conserved in mammals. In particular, we simultaneously knocked out close paralogs, and by so doing we succeeded in demonstrating functional redundancy among some of these paralogs. As an example, we provided evidence that Rab1A/B and Rab5A/B/C are redundantly required for cell survival and growth, respectively (Fig. 1). On the other hand, previous genome-wide KO screenings seeking "essential" (needed for cell growth and/or survival) genes failed to identify Rab1 and Rab5 as essential genes (Blomen et al., 2015; Wang et al., 2015), which in turn highlights the advantage of our KO strategy. The previous studies also showed that genes that have paralogs tend to be nonessential. These facts emphasize the importance of careful analysis of specific sets of genes (e.g., Rab family genes) with consideration of functional redundancy, even in the era of powerful genome-wide KO screening. Thus, our Rab-KO cells are valuable resources that will benefit a wide range of membrane trafficking research.

Roles of Rabs in organelle homeostasis

Immunofluorescence analysis of Rab-KO cells validated previously proposed roles of several Rabs in organelle homeostasis (Figs. 2 and S3). Rab2 is thought to be involved in ER-to-Golgi transport and Golgi organization (Tisdale et al., 1992; Aizawa and Fukuda, 2015). Based on our results, however, Rab2 is unlikely to be critical for protein secretion, because Rab2-KO cells formed the basement membrane normally (Fig. 3) and because the band pattern of secreted proteins in the medium appeared not to differ from the pattern in the medium of parental cells (not depicted). By contrast, we showed that loss of Rab2 induces fragmentation and dispersion of the Golgi. Golgi-localized Rab2 effectors, such as GMAP210, golgin-45, and GARI-L4 (Short et al., 2001; Gillingham et al., 2014; Aizawa and Fukuda, 2015; Sato et al., 2015), are likely to be involved in this phenotype. We found that Rab6 is also required for Golgi homeostasis. The dilation of the Golgi upon loss of Rab6 was consistent with a previous report, although no increased continuity was observed, at least in our Rab6-KO cells (Storrie et al., 2012). By contrast, the decreased GalNT2 staining observed in Rab6-KO cells was somewhat unexpected in view of the previously suggested function of Rab6, that is, of mediating the Golgi-to-ER retrieval of Golgi enzymes such as GalNT2 (Girod et al., 1999). Further investigation is needed to determine the exact role of Rab6 in Golgi homeostasis.
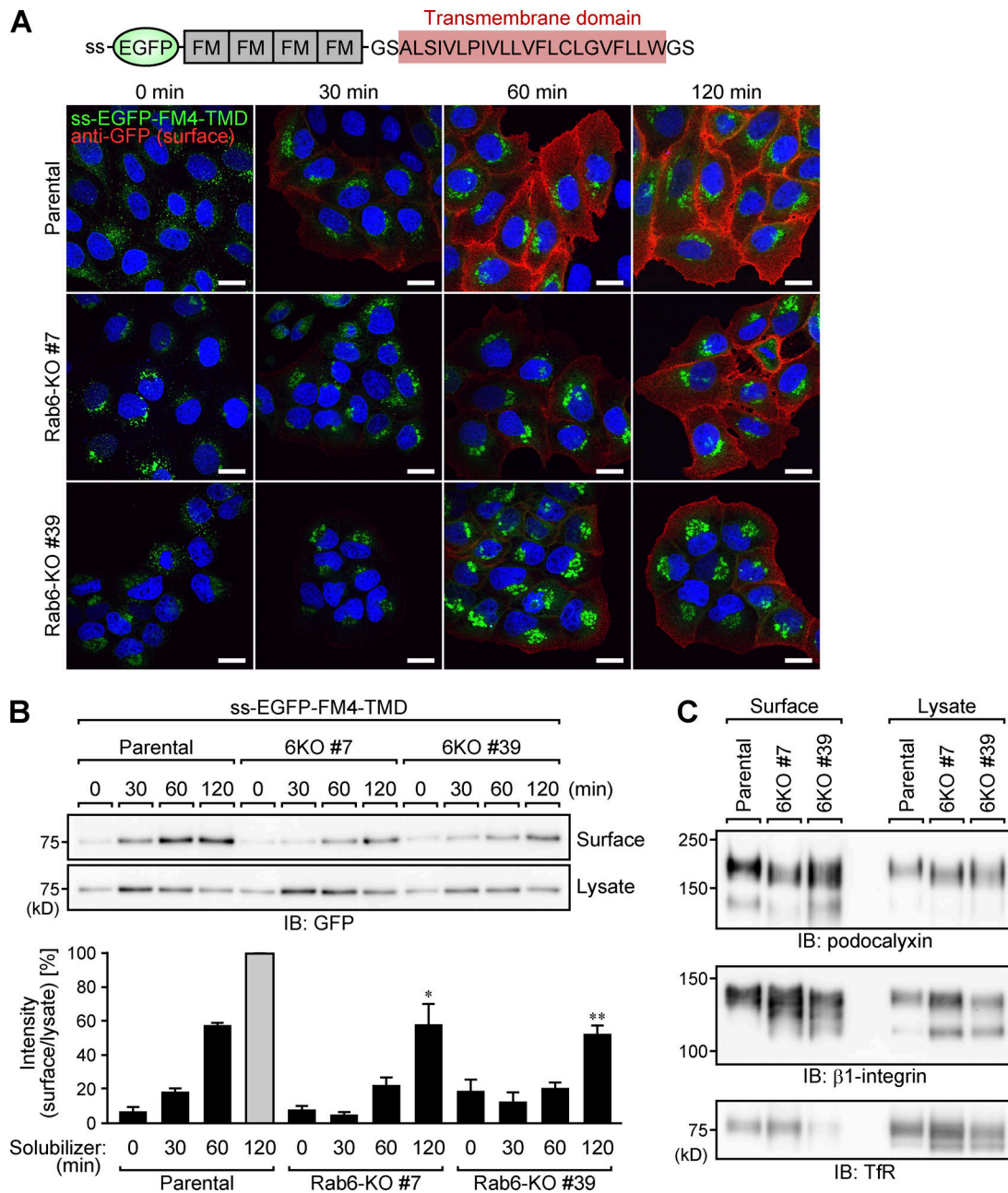
Figure 5. **Secretion kinetics of transmembrane proteins in parental and Rab6-KO cells. (A and B)** Secretion kinetics of ss-EGFP-FM4-TM in parental and Rab6-KO cells. Parental and Rab6-KO cells that stably express ss-EGFP-FM4-TM were treated with 250 µM D/D solubilizer to trigger synchronized transport of the cargo to the plasma membrane. After 0, 30, 60, and 120 min, the externalized cargo was labeled with an anti-GFP antibody (red) on ice for 20 min, and the cells were then fixed with PFA (DAPI in blue). Scale bars, 20 µm (A). The externalized cargo was also labeled by surface biotinylation, then collected with streptavidin beads after cell lysis, and immunoblotted (IB) with an anti-GFP antibody. The graph represents quantification of the band intensities normalized to that of parental cells (120 min). Data are means and SEM. The amount of the biotinylated cargo at 120 min was statistically analyzed. *, P < 0.05; **, P < 0.01 (n = 3, Dunnett's test). **(C)** Steady-state amount of the cell surface proteins of parental and Rab6-KO cells. Total cell surface proteins of parental and Rab6-KO cells were biotinylated and then collected with streptavidin beads after cell lysis. The samples were analyzed by immunoblotting with anti-podocalyxin, anti–β1-integrin, and anti-TfR antibodies.

We showed that loss of Rab7A induces enlarged lysosomes and cathepsin B leakage into the extracellular space. These phenotypes can be explained by the fact that Rab7A interacts with and recruits a retromer subcomplex, Vps26–Vps29–Vps35 (Rojas et al., 2008), and that the retromer is required for endosome-to-Golgi retrieval of M6PR, the main sorting receptor for lysosomal enzymes (Seaman, 2004). Although Vps35 remained on endosomes in Rab7A-KO cells, the Vps35-labeled endosomes, which were mostly separated from lysosomes, were also enlarged (Fig. 2 C), indicating dysregulation of the retromer complex. It has been reported that Rab9 mediates M6PR transport from endosomes to the Golgi and that
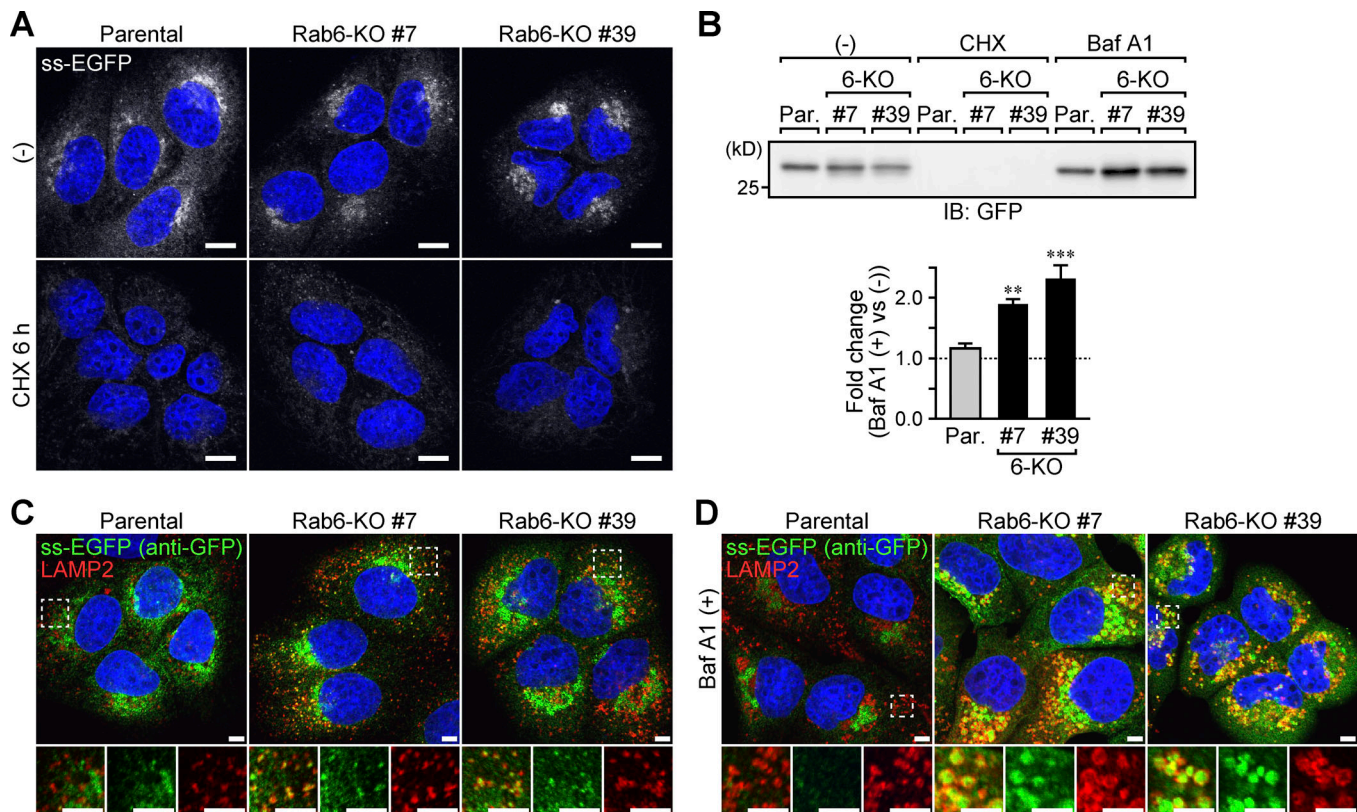
Figure 6. **Unsecreted ss-EGFP is mistargeted to lysosomes in Rab6-KO cells. (A)** CHX chase of ss-EGFP. Parental and Rab6-KO cells that stably express ss-EGFP were treated with 100 ng/ml CHX for 0 and 6 h and then fixed with PFA (DAPI in blue). Scale bars, 10 μm. **(B)** Effect of CHX or BafA1 treatment on the amount of intracellular ss-EGFP. Parental and Rab6-KO cells that stably express ss-EGFP were treated with 100 ng/ml CHX or 100 nM BafA1 for 0 and 6 h. The cell lysates were analyzed by immunoblotting (IB) with an anti-GFP antibody. The graph shows fold changes in the band intensities after treatment with BafA1 in comparison with band intensities before treatment. **, P < 0.01; ***, P < 0.001 (n = 4; Dunnett's test). **(C and D)** Immunostaining of ss-EGFP and lysosomes. Parental and Rab6-KO cells that stably express ss-EGFP were untreated (C) or treated with BafA1 for 10 h (D), fixed with PFA, and then immunostained with anti-GFP (green) and anti-LAMP2 (red) antibodies (DAPI in blue). Scale bars, 5 μm. The lower panels show the magnified views of the boxed areas in the upper panels. See also Fig. S6.

expression of a constitutively negative form of Rab9 suppresses this traffic, resulting in secretion of lysosomal enzymes (Riederer et al., 1994). However, our Rab9-KO cells showed neither lysosomal defects nor extracellular secretion of lysosomal enzymes. Instead, we demonstrated that combinatorial KO of Rab7A and Rab9 led to more severely enlarged lysosomes than observed in Rab7A-KO cells, indicating that Rab9 is not essential for, but backs up, retrieval of M6PR from endosomes to the Golgi. Since, as far as we know, Rab7A and Rab9 interact with completely different effectors (Fukuda et al., 2008; Matsui et al., 2012), they should regulate M6PR transport via different mechanisms. Thus, expanding the combination of simultaneous KO sets from closely related genes (e.g., Rab1A and B, whose products can bind to the same effectors) to more distant yet related genes (e.g., Rab7A and Rab9, whose products bind different effectors) would reveal unexpected functional interactions of Rab-mediated membrane trafficking. To extend our KO study with this view, we further generated additional combinatorial KO cells (i.e., Rab7A/B-KO, Rab11/25-KO, Rab19/43-KO, Rab26/37-KO, Rab34/36-KO, and Rab39/42-KO cells) for potential paralogs suggested by an evolutionary study of the Rab family (Klöpper et al., 2012) and added them to our KO cell

collection (Table S1). The images of organelle staining of these cells are available from BioStudies (Extended Figs. S2 and S3), although no obvious abnormality was observed for organelle staining of these KO cells at this stage. Future extensive research will clarify the exact phenotypes of these combinatorial KO cells.

Since MDCK cells can be applied not only to polarized transport assays but to general membrane trafficking assays, such as for endocytic, recycling, and retrograde pathways, our Rab-KO cell collection would be quite useful for analyzing these membrane trafficking routes. In addition, analyzing other organelles, such as peroxisomes, mitochondria, lipid droplets, and autophagosomes, would be worthwhile in the future.

Roles of Rabs in epithelial morphogenesis

Self-organization of epithelial cells into spherical hollow cysts when embedded in ECM gels is an excellent model for investigating epithelial polarization and morphogenesis. We comprehensively screened for Rabs that are essential to this process by culturing Rab-KO MDCK cells in collagen-I gels, and the results showed that only Rab11-KO cells substantially formed cysts with multiple small lumens (Figs. 4 A and S4). In epithelial cells, Rab11 and its effectors such as myosin Vb and Rab11 family interacting

proteins localize to apical recycling endosomes and are required for recycling and the secretory route toward the apical surface (Goldenring, 2015). Although the function of Rab11 has previously been investigated by knockdown or overexpressing a dominant-negative form of Rab11 or by generating Rab11A-KO mice (Sobajima et al., 2014; Yu et al., 2014), this is the first time that both Rab11A and B have been knocked out in mammalian cells. Indeed, KO of Rab11A alone was insufficient to result in the multilumen phenotype in MDCK cells (Fig. S5 A), and the Rab11A/B-KO phenotype was rescued by expressing Rab11A alone (Fig. 4 A), leading us to conclude that Rab11A and B redundantly function in the creation of a proper single lumen. It should be noted that ezrin and E-cadherin were correctly localized on apical and basolateral membranes, respectively, indicating that polarity formation itself is not impaired, even in Rab11-KO cells. Although Rab8 depletion has also been shown to lead to multiple lumen formation (Bryant et al., 2010; Vogel et al., 2015; Mrozowska and Fukuda, 2016), our Rab8-KO cells, at least, did not recapitulate this phenotype. This discrepancy could be explained by the fact that adaptation to long-term depletion occasionally masks the potential involvement of a certain gene in a specific phenotype. In fact, Rab8-KO mice showed a defect in apical trafficking only in their intestinal epithelia (Sato et al., 2014), indicating that other Rabs such as Rab10 and Rab13, which share several effectors with Rab8 (Fukuda et al., 2008; Rai et al., 2016), can compensate for Rab8 function in tissues other than intestine when Rab8 has been stably knocked out. Rab3, Rab25, and Rab27 have also been implicated in single lumen formation previously (Bryant et al., 2010; Gálvez-Santisteban et al., 2012), but their KO did not result in any severe abnormalities in our screening. Similar scenarios as that of Rab8 may be applicable to these Rabs, and future detailed comparison between acute versus long-term depletion is needed to clarify this issue.

We also investigated another characteristic of epithelia, their basement membrane, which provides epithelial cells with polarity cues and physical linkage to the underlying connective tissue that protects them from mechanical stress (Yurchenco, 2011). The results of the immunofluorescence screening for laminin, a major basement membrane component, showed that the Rab6-KO cysts did not form the basement membrane (Figs. 3 and 4 B). This result was consistent with the previous finding that Rab6A-KO mice were lethal at embryonic day 5.5–6 and that the embryos lacked the basement membrane (Shafaq-Zadah et al., 2016). While the authors of that study concluded that Rab6-dependent retrograde transport of β1-integrin is required for basement membrane formation, our data suggested another nonexclusive possibility, that inability to secrete ECM components is the reason for the lack of the basement membrane.

Rab6 is required for the secretory pathway
By using quantitative mass spectrometry, we provided evidence that secretion of other secretory proteins as well as ECM components is globally inhibited in Rab6-KO cells (Fig. 4 F). In the previous studies, the effect of Rab6A depletion on the secretory pathway was assessed by using VSVG as a model cargo, and Golgi-to-plasma-membrane, but not ER-to-Golgi, transport of

VSVG was shown to be delayed in Rab6A knockdown cells (Grigoriev et al., 2007; Miserey-Lenkei et al., 2010; Storrie et al., 2012; Johns et al., 2014). By contrast, requirement of Rab6 for secretion of soluble cargos is somewhat controversial, because secretion of ss-GFP-FM4-FCS-hGH was decreased by Rab6A knockdown, whereas secretion of neuropeptide Y and Gaussia luciferase were unaffected (Grigoriev et al., 2007, 2011; Johns et al., 2014). This discrepancy may be attributable to the difference in cargo-specific sorting signals or in the expression level of Rab6B, which can compensate for the function of Rab6A (Fig. 4 D). To avoid any cargo-specific sorting, we used ss-EGFP as a model of soluble secretory cargos and demonstrated that secretion of ss-EGFP was remarkably inhibited in Rab6-KO cells (only ~25% of that of parental cells; Fig. 4 G). We also reassessed the effect of loss of Rab6 on transport of transmembrane proteins by using a transmembrane model cargo with no cytoplasmic domain, ss-EGFP-FM4-TM, instead of VSVG, because the cytoplasmic tail of VSVG is known to undergo regulation by clathrin adaptor complex AP-1 and coatomer complex COPI (Fölsch et al., 2003; Park et al., 2015). The results showed that the efficiency of surface delivery of the transmembrane cargo in Rab6-KO cells was nearly halved, which is quite consistent with the previous data obtained with VSVG (Fig. 5, A and B). Our findings that transport of soluble cargos is more dependent on Rab6 than transport of transmembrane cargos suggest that another compensatory pathway exists for transmembrane cargos, or that soluble cargos and transmembrane cargos are differently regulated during their anterograde transport. Since a previous report indicated that soluble cargos and transmembrane cargos in hepatocytes are mostly segregated into different post-Golgi vesicles (Saucan and Palade, 1994), such sorting may also occur in MDCK cells. Whether it actually does awaits further investigation.

We also demonstrated that unsecreted cargos, including endogenous laminin and exogenous ss-EGFP, in Rab6-KO cells are delivered to lysosomes for degradation (Fig. 6, C and D; and Fig. S6 B), suggesting that cells naturally eliminate excess secretory vesicles so that cells are not to be filled up with unsecreted cargos.

Which steps in the secretory pathway are inhibited in Rab6-KO cells? CHX chase of ss-EGFP revealed that even in Rab6-KO cells, ss-EGFP rapidly disappears from the Golgi after CHX treatment (Fig. 6 A), indicating that anterograde transport is not impaired until exit from the Golgi. We therefore hypothesized that transport and/or fusion of post-Golgi vesicles to the plasma membrane is inhibited in Rab6-KO cells. If so, the most likely candidate effectors of Rab6 would be Bicaudal D and ELKS, which have been reported to mediate transport and tethering, respectively, of Rab6-containing post-Golgi vesicles to the plasma membrane (Grigoriev et al., 2007). However, we found that neither ELKS1/2-KO nor Bicaudal D1/D2-KO cysts had any defects in ECM formation (Fig. S6, C–E), indicating that they are not responsible for the secretory defect of Rab6-KO cells. Future investigation of other Rab6 effectors, including as yet unidentified Rab effectors, will be necessary to clarify the precise mechanism of the Rab6-mediated transport of secretory cargos.

Materials and methods

Cell lines

MDCK cells (strain II; from a kidney of a female cocker spaniel) were grown in culture medium (DMEM; Fujifilm Wako Pure Chemical; 044-29765) supplemented with 10% FBS, 100 µg/ml streptomycin (Meiji Seika Pharma), and 100 U/ml penicillin G (Meiji Seika Pharma) at 37°C under 5% CO_2. Although our MDCK cells have not been authenticated, we confirmed that they have a low transepithelial resistance value (<300 Ω·cm², typical of MDCK strain II; Yasuda et al., 2012). Plat-E cells (derivative of HEK293T [female] cells) were a gift from Dr. Toshio Kitamura (The University of Tokyo, Tokyo, Japan). They were grown in the same culture medium and used for retrovirus production.

Antibodies

Rabbit polyclonal anti-Rab antibodies (1A, 1B, 2A, 2B, 3D, 4A, 4B, 5A, 5B, 5C, 6A, 7A, 13, 14, 15, 18, 19, 20, 21, 22A, 24, 27A, 30, 32, 33B, 34, and 39A/B) were raised against GST-Rabs (Itoh et al., 2008) and affinity purified from the antiserum as follows. A crude IgG fraction was obtained by ammonium sulfate precipitation. The precipitate was dissolved in and dialyzed against PBS. The possible GST-recognizing antibody was removed by passing through a GST-bound glutathione-Sepharose column, and the flowthrough was incubated with antigen-bound Affi-Gel 10 beads (Bio-Rad; 1536099). The column was washed with 10 mM Hepes-KOH, pH 7.2, and the anti-Rab IgG bound to the beads was eluted with an elution buffer (0.2 M glycine-HCl, pH 2.8, and 1 mM EDTA). The eluate was quickly neutralized with 1 M Tris base, dialyzed against PBS, and concentrated by using Centriprep 30K (Merck Millipore). An anti-podocalyxin antibody was prepared by the same protocol (Mrozowska and Fukuda, 2016). The other antibodies were obtained commercially (Table S3).

Plasmid construction

All Cas9-encoding vectors used in this study were constructed from the previously reported pSpCas9(BB)-2A-Puro vector (Ran et al., 2013). The sequences of the insert oligonucleotides were chosen by using a web tool (CRISPRdirect; Naito et al., 2015) and are shown in Table S1. The pMRX-IRES-puro retroviral vector was a gift from Dr. Shoji Yamaoka (Tokyo Medical and Dental University, Tokyo, Japan; Saitoh et al., 2003). cDNAs of EGFP-tagged mouse Rab1B, Rab6A, and Rab11A (Itoh et al., 2006) were inserted into the pMRX-IRES-puro vector. cDNAs of Myc-tagged mouse Rab2A, Rab2B, and Rab5A (Itoh et al., 2006) were inserted into the pMRX-IRES-bsr vector, in which a puromycin resistance gene of the pMRX-IRES-puro vector had been replaced by a blasticidin S resistance gene. The National Center for Biotechnology Information accession numbers of all of the mouse Rab genes mentioned above are described in Itoh et al. (2006). To generate retroviruses encoding secretory and transmembrane forms of EGFP, EGFP that had been fused to a signal sequence of calreticulin (mouse NM_007591) was inserted into the pMRX-IRES-bsr vector (named pMRX-bsr ss-EGFP), and then four FM domains were fused in tandem (Hirano et al., 2016) to the ss-EGFP (named pMRX-bsr ss-EGFP-FM4). Finally, the transmembrane domain of LDL receptor (human NM_000527)

was fused to the ss-EGFP-FM4 (named pMRX-bsr ss-EGFP-FM4-TM). All plasmids constructed in this study have been deposited in the RIKEN Bioresource Center (https://dnaconda.riken.jp/search/depositor/dep005893.html). pLP-VSVG was obtained from Thermo Fisher Scientific (K497500). pGEX-6P-1-GFP nanobody was a gift from Dr. Kazuhisa Nakayama (Kyoto University, Kyoto, Japan; Katoh et al., 2015).

Retrovirus production and infection into MDCK cells

Plat-E cells (Morita et al., 2000) were plated on a 35-mm dish at 2×10^5 cells/dish and transfected with 2 µg of pMRX plasmids together with 1 µg pLP-VSVG. After 24 h, the medium was changed, and the cells were cultured for an additional 24 h. The medium was collected and centrifuged at 11,000 g for 2 min to remove debris. This virus-containing medium was added to the culture medium of MDCK cells in the presence of 4 µg/ml polybrene, and after 48 h the transformants were selected by 2 µg/ml puromycin (Merck) or 10 µg/ml blasticidin S (Fujifilm Wako Pure Chemical) for 24–48 h. Only Rab5A/B-KO cells could not be selected well with retrovirus, and as a result we obtained a mixture of cells, about half of which expressed Myc-Rab5A.

Generation of KO cells

MDCK cells were transfected with single guide RNA/Cas9-encoding plasmids, and the transfected cells were selected in 2 µg/ml puromycin for 24 h. The cells were then cloned by limiting dilution, and each clone was checked for target gene disruption by genomic PCR followed by sequencing of the product (Extended Figs. S1 and S4 in BioStudies). Loss of target protein expression in many of the Rab-KO cell lines was also validated by immunoblotting (indicated in the KO check by immunoblotting column of Table S1 and Fig. S1).

Genomic PCR and sequencing

Cells were lysed in a digestion buffer (0.5% SDS, 100 mM NaCl, 10 mM Tris-HCl, pH 8.0, 25 mM EDTA, pH 8.0, and 0.1 mg/ml proteinase K) and incubated at 50°C for 3 h. An equal volume of phenol/chloroform was added to the lysate, which was vortexed and then centrifuged at 1,700 g for 3 min. The genomic DNA in the supernatant was ethanol precipitated and then subjected to a PCR reaction. The target sequence and its surrounding region (∼500 bp) in the genome was amplified using LA Taq (Takara Bio) and appropriate primers (shown in Table S1), and the product was directly sequenced using either of the primers.

Fluorescence microscopy

For immunostaining, cells were fixed with either 4% PFA for 30 min or 10% TCA for 10 min, permeabilized with 0.2% Triton X-100/PBS for 3 min, and blocked with 1% BSA/PBS for 30 min. The cells were then sequentially incubated for 1 h each with primary and Alexa Fluor–conjugated secondary antibodies diluted in 1% BSA/PBS. The dilutions of the primary antibodies were: Vps35 (1:300), EEA1 (1:300), ezrin (1:300), LAMP2 (1:500), Myc (1:500), TfR (1:300), GalNT2 (1:300), GFP (1:2,000), laminin (1:300), reticulon 4 (1:300), and E-cadherin (1:300). Cysts were finally suspended in PBS and placed on a glass-bottomed dish for microscopy. Fluorescence images were obtained by using

Homma et al.
Comprehensive Rab knockout in epithelial cells

Journal of Cell Biology 2046
https://doi.org/10.1083/jcb.201810134

FluoView software and a FV1000 confocal laser-scanning microscope (Olympus) equipped with a Plan-Apochromat 63×/1.4 oil-immersion objective lens and an electron-multiplying charge-coupled device camera (C9100; Hamamatsu Photonics). Cropping and level adjustment of the images were performed in Photoshop CS6 software (Adobe).

Immunoblotting

Denatured proteins in an SDS sample buffer (62.5 mM Tris-HCl, pH 6.8, 2% 2-mercaptoethanol, 2% SDS, 10% glycerol, and 0.02% bromophenol blue) were resolved by SDS-PAGE and transferred to polyvinylidene difluoride membranes (Merck Millipore). The membranes were blocked for 30 min with 1% skimmed milk/PBS containing 0.1% Tween-20 (PBS-T) and incubated for 1 h with appropriate primary antibodies diluted in the blocking solution. The membranes were then washed three times with PBS-T and incubated for 1 h with HRP-conjugated secondary antibodies diluted in the blocking solution. Chemiluminescence signals were detected by using an ECL substrate (Bio-Rad; 1705060) and x-ray films or a chemiluminescence imager (ChemiDoc Touch; Bio-Rad), and band intensity was quantified using Image Lab software (Bio-Rad).

Knockdown experiments

For Rab1A knockdown, cells were plated in a 12-well plate at 10^4 cells/well and transfected with 10 nM siControl or siRab1A (#1 or #3). After 72 h, the cells were trypsinized and counted. For Rab5C knockdown, Rab5A/B-KO cells, about half of which express Myc-Rab5A, were plated in a 12-well plate at 10^4 cells/well and transfected with siControl or siRab5C (#1 or #2). After 72 h, the cells were replated and again transfected with the same siRNAs. This cycle was repeated three times, and the number of Myc-Rab5A(−) cells per 100 cells at each passage was counted after immunostaining. The sequences of siRNAs used in this study are listed in Table S3.

Collagen culture for 3D cyst formation

Cells were trypsinized and resuspended in culture medium containing 12 mM Hepes, pH 7.2, and 2 mg/ml collagen I. This mixture was placed in a 24-well plate, added with 2 ml of the culture medium, and cultured for 7 d. After removing the medium, 10% TCA was added to lyse the gel and fix the cells, and they were immunostained.

Analysis of ECM proteins

Cells were plated on a 35-mm dish at 2×10^5 cells/dish. The next day, the cells were washed three times with PBS, and after incubating with 20 mM ammonium hydroxide for 10 min, the lysed cells were removed by washing with PBS. The remaining ECM proteins in the dish were dissolved in the SDS sample buffer. The samples were analyzed by immunoblotting.

Analysis of total secreted proteins

Cells were plated on a 35-mm dish at 2×10^5 cells/dish. The next day, the cells were washed three times with FBS(−) DMEM to reduce contamination by serum proteins, and the medium was replaced by the serum-free medium (OptiPRO SFM supplemented with 4 mM L-glutamine; Thermo Fisher Scientific) to allow cells to secrete proteins for 18 to 24 h. The medium was collected in a 1.5-ml tube and centrifuged at 11,000 g for 2 min, and the supernatant was concentrated by freeze-drying. The dried samples were then diluted in 40 µl of Milli-Q (Merck Millipore) and desalted with Sephadex G-25 beads (GE Healthcare), and 10 µl of 5× sample buffer was added. The samples were analyzed by immunoblotting.

Quantitative proteomics

Parental and Rab6-KO cells (#7) were cultured on permeable filters in six-well plates for 3 d after reaching confluence. The cells were washed three times with FBS(−) DMEM, and the medium was replaced with the serum-free medium. After 18 h, the serum-free medium was collected and replenished to allow cells to secrete proteins for an additional 18 h. The proteins secreted from the apical and basal chamber for 36 h (∼15 ml in total) were centrifuged at 11,050 g for 5 min to remove debris and then collectively concentrated to ∼1 ml by using Centriprep 10K (Merck Millipore). The buffer was replaced with 0.5 M triethylammonium bicarbonate, pH 8.5, by using Vivaspin 6-5K (GE Healthcare). Equal volumes (131 µl) of concentrated samples (parental: 130.0 µg, Rab6-KO: 70.5 µg) were further concentrated in a centrifugal evaporator and then diluted in 26 µl of 0.5 M triethylammonium bicarbonate, pH 8.5. The samples were reduced by adding 2% SDS (1/20 volume) and 50 mM Tris(2-carboxyethyl)phosphine (1/10 volume) and incubating at 60°C for 2 h. Free thiols were then blocked by adding 200 mM methyl methanethiosulfonate (1/20 volume) and incubating at 25°C for 30 min. The proteins were digested by sequentially adding 1 µg/µl trypsin (Sciex; 4352157; 1/20 volume at 37°C for 5 h, 1/20 volume at 37°C for 15 h, and finally 1 µl at 37°C for 4 h). The samples were desalted by using a Sep-Pak Light C18 Cartridge (Waters; WAT023501). The peptides then were labeled by using an iTRAQ Reagent-multiplex Assay Kit (Sciex; 4390812) at 25°C for 2 h. The labeled samples were mixed and fractionated by strong cation exchange using a Cation Exchange Buffer Pack (Sciex; 4326747), which yielded three fractions. The fractions were desalted and concentrated by using a Sep-Pak Light C18 Cartridge and a centrifugal evaporator, respectively. The samples were diluted in 30 µl of solution A (5% acetonitrile and 0.1% formic acid), and after centrifugation at 10,000 g for 1 min, the supernatants were used for mass spectrometry. Mass spectrometry was performed by using a Sciex TripleTOF 5600 system and DiNa system (KYA Technologies), and the mass spectrometry and tandem mass spectrometry data were analyzed by using ProteinPilot Software 4.5 (Sciex).

Analysis of ss-EGFP secretion

Parental and Rab6-KO cells that stably express ss-EGFP were plated on 35-mm dishes at 2×10^5 cells/dish. The next day, the cells were washed with the culture medium and allowed to secrete ss-EGFP into the culture medium for 6 h. The medium was collected and centrifuged at 11,000 g for 2 min to remove debris, and the supernatants were rotated overnight at 4°C with 5 µg of GST-GFP nanobody and 12 µl of glutathione-Sepharose beads (GE Healthcare). The beads were washed with PBS three times and boiled in the SDS sample buffer. The samples were analyzed

by immunoblotting. The amounts of ss-EGFP in the medium were normalized to the amounts in the lysates.

Purification of GST-GFP nanobody
Escherichia coli JM109 was transformed with pGEX-6P-1-GFP-Nanobody, and expression was induced with 1 mM isopropyl β-D-1-thiogalactopyranoside for 3 h. Cells were centrifuged at 3,410 g for 5 min and resuspended in a buffer (150 mM NaCl, 16 mM Na_2HPO_4, 40 mM $NaH_2PO_4 \cdot 2H_2O$, and 0.1 mM phenyl-methylsulfonyl fluoride), and then sonicated and lysed with 1% (final concentration) Triton X-100/PBS for 15 min. The lysate was centrifuged at 11,050 g for 15 min, and GST-GFP nanobody in the supernatant was trapped with glutathione-Sepharose beads. The beads were washed with PBS three times and eluted with 5 mM glutathione in 50 mM Tris-HCl, pH 8.0. The eluate was dialyzed against PBS and concentrated by using Centriprep 10K.

Surface biotinylation
For surface biotinylation, cells were washed with cold PBS(+) (PBS containing 0.1 mM $CaCl_2$ and 0.1 mM $MgCl_2$) three times and incubated with 0.2 mg/ml Sulfo-NHS-biotin in PBS(+) for 20 min on ice. The cells were then washed with cold PBS(+) three times and lysed with a lysis buffer (50 mM Tris-HCl, pH 7.5, 150 mM NaCl, 1% Triton X-100, 10% glycerol, 100 mM $MgCl_2$, 1 mM dithiothreitol, and 1× protease inhibitor [cOmplete; Sigma-Aldrich]). The lysate was centrifuged at 17,400 g for 10 min, and the supernatant was incubated with 5 μl of strep-tavidin agarose for 2 h. The beads were washed with the lysis buffer three times and boiled in the SDS sample buffer. The samples were analyzed by immunoblotting.

Quantification and statistical analysis
All quantitative data are expressed as the means and SEM (except in Fig. 4 F, in which raw data are plotted by box plot and the median values). Tukey's test and Dunnett's test were performed on R software, and the following significance levels were used: *, $P < 0.05$; **, $P < 0.01$; and ***, $P < 0.001$.

Online supplemental material
Fig. S1 shows endogenous Rab expression in MDCK cells and its loss in Rab-KO cells. Fig. S2 shows expression and localization of mutant Rab4A, Rab10, and Rab22A proteins that have one amino acid deletion. Fig. S3 shows immunofluorescence analysis of the ER, Golgi, early endosomes, recycling endosomes, and lysosomes in Rab-KO cells. Fig. S4 shows immunostaining of ezrin and E-cadherin in Rab-KO cysts. Fig. S5 shows that Rab6 and Rab11 are required for normal epithelial morphogenesis. Fig. S6 shows analysis of the secretory defect in Rab6-KO cells. Table S1 is a list of the KO cells. Table S2 is a list of the proteins identified by quantitative mass spectrometry. Table S3 is a list of the materials used in this article.

Acknowledgments

References

Aizawa, M., and M. Fukuda. 2015. Small GTPase Rab2B and its specific binding protein Golgi-associated Rab2B interactor-like 4 (GARI-L4) regulate Golgi morphology. *J. Biol. Chem.* 290:22250–22261. https://doi.org/10.1074/jbc.M115.669242

Blomen, V.A., P. Májek, L.T. Jae, J.W. Bigenzahn, J. Nieuwenhuis, J. Staring, R. Sacco, F.R. van Diemen, N. Olk, A. Stukalov, et al. 2015. Gene essentiality and synthetic lethality in haploid human cells. *Science.* 350:1092–1096. https://doi.org/10.1126/science.aac7557

Bryant, D.M., A. Datta, A.E. Rodríguez-Fraticelli, J. Peränen, F. Martín-Belmonte, and K.E. Mostov. 2010. A molecular network for *de novo* generation of the apical surface and lumen. *Nat. Cell Biol.* 12:1035–1045. https://doi.org/10.1038/ncb2106

Cong, L., F.A. Ran, D. Cox, S. Lin, R. Barretto, N. Habib, P.D. Hsu, X. Wu, W. Jiang, L.A. Marraffini, and F. Zhang. 2013. Multiplex genome engineering using CRISPR/Cas systems. *Science.* 339:819–823. https://doi.org/10.1126/science.1231143

Delprato, A., E. Merithew, and D.G. Lambright. 2004. Structure, exchange determinants, and family-wide Rab specificity of the tandem helical bundle and Vps9 domains of Rabex-5. *Cell.* 118:607–617. https://doi.org/10.1016/j.cell.2004.08.009

Feig, L.A. 1999. Tools of the trade: use of dominant-inhibitory mutants of Ras-family GTPases. *Nat. Cell Biol.* 1:E25–E27. https://doi.org/10.1038/10018

Fölsch, H., M. Pypaert, S. Maday, L. Pelletier, and I. Mellman. 2003. The AP-1A and AP-1B clathrin adaptor complexes define biochemically and functionally distinct membrane domains. *J. Cell Biol.* 163:351–362. https://doi.org/10.1083/jcb.200309020

Fukuda, M. 2008. Regulation of secretory vesicle traffic by Rab small GTPases. *Cell. Mol. Life Sci.* 65:2801–2813. https://doi.org/10.1007/s00018-008-8351-4

Fukuda, M., T.S. Kuroda, and K. Mikoshiba. 2002. Slac2-a/melanophilin, the missing link between Rab27 and myosin Va: implications of a tripartite protein complex for melanosome transport. *J. Biol. Chem.* 277:12432–12436. https://doi.org/10.1074/jbc.C200005200

Fukuda, M., E. Kanno, K. Ishibashi, and T. Itoh. 2008. Large scale screening for novel Rab effectors reveals unexpected broad Rab binding specificity. *Mol. Cell. Proteomics.* 7:1031–1042. https://doi.org/10.1074/mcp.M700569-MCP200

Gálvez-Santisteban, M., A.E. Rodriguez-Fraticelli, D.M. Bryant, S. Vergarajauregui, T. Yasuda, I. Bañón-Rodríguez, I. Bernascone, A. Datta, N. Spivak, K. Young, et al. 2012. Synaptotagmin-like proteins control the formation of a single apical membrane domain in epithelial cells. *Nat. Cell Biol.* 14:838–849. https://doi.org/10.1038/ncb2541

Gillingham, A.K., R. Sinka, I.L. Torres, K.S. Lilley, and S. Munro. 2014. Toward a comprehensive map of the effectors of Rab GTPases. *Dev. Cell.* 31:358–373. https://doi.org/10.1016/j.devcel.2014.10.007

Girod, A., B. Storrie, J.C. Simpson, L. Johannes, B. Goud, L.M. Roberts, J.M. Lord, T. Nilsson, and R. Pepperkok. 1999. Evidence for a COP-I-independent transport route from the Golgi complex to the endoplasmic reticulum. *Nat. Cell Biol.* 1:423–430. https://doi.org/10.1038/15658

Goldenring, J.R. 2015. Recycling endosomes. *Curr. Opin. Cell Biol.* 35:117–122. https://doi.org/10.1016/j.ceb.2015.04.018

Grigoriev, I., D. Splinter, N. Keijzer, P.S. Wulf, J. Demmers, T. Ohtsuka, M. Modesti, I.V. Maly, F. Grosveld, C.C. Hoogenraad, and A. Akhmanova. 2007. Rab6 regulates transport and targeting of exocytotic carriers. *Dev. Cell.* 13:305–314. https://doi.org/10.1016/j.devcel.2007.06.010

Grigoriev, I., K.L. Yu, E. Martinez-Sanchez, A. Serra-Marques, I. Smal, E. Meijering, J. Demmers, J. Peränen, R.J. Pasterkamp, P. van der Sluijs, et al. 2011. Rab6, Rab8, and MICAL3 cooperate in controlling docking and fusion of exocytotic carriers. *Curr. Biol.* 21:967–974. https://doi.org/10.1016/j.cub.2011.04.030

Hirano, S., T. Uemura, H. Annoh, N. Fujita, S. Waguri, T. Itoh, and M. Fukuda. 2016. Differing susceptibility to autophagic degradation of two LC3-binding proteins: SQSTM1/p62 and TBC1D25/OATL1. *Autophagy.* 12:312–326. https://doi.org/10.1080/15548627.2015.1124223

Homma, Y., and M. Fukuda. 2016. Rabin8 regulates neurite outgrowth in both GEF activity-dependent and -independent manners. *Mol. Biol. Cell.* 27:2107–2118. https://doi.org/10.1091/mbc.E16-02-0091

Hutagalung, A.H., and P.J. Novick. 2011. Role of Rab GTPases in membrane traffic and cell physiology. *Physiol. Rev.* 91:119–149. https://doi.org/10.1152/physrev.00059.2009

Itoh, T., M. Satoh, E. Kanno, and M. Fukuda. 2006. Screening for target Rabs of TBC (Tre-2/Bub2/Cdc16) domain-containing proteins based on their Rab-binding activity. *Genes Cells.* 11:1023–1037. https://doi.org/10.1111/j.1365-2443.2006.00997.x

Itoh, T., N. Fujita, E. Kanno, A. Yamamoto, T. Yoshimori, and M. Fukuda. 2008. Golgi-resident small GTPase Rab33B interacts with Atg16L and modulates autophagosome formation. *Mol. Biol. Cell.* 19:2916–2925. https://doi.org/10.1091/mbc.e07-12-1231

Johns, H.L., C. Gonzalez-Lopez, C.L. Sayers, M. Hollinshead, and G. Elliott. 2014. Rab6 dependent post-Golgi trafficking of HSV1 envelope proteins to sites of virus envelopment. *Traffic.* 15:157–178. https://doi.org/10.1111/tra.12134

Katoh, Y., S. Nozaki, D. Hartanto, R. Miyano, and K. Nakayama. 2015. Architectures of multisubunit complexes revealed by a visible immunoprecipitation assay using fluorescent fusion proteins. *J. Cell Sci.* 128:2351–2362. https://doi.org/10.1242/jcs.168740

Klöpper, T.H., N. Kienle, D. Fasshauer, and S. Munro. 2012. Untangling the evolution of Rab G proteins: implications of a comprehensive genomic analysis. *BMC Biol.* 10:71. https://doi.org/10.1186/1741-7007-10-71

Kuchitsu, Y., Y. Homma, N. Fujita, and M. Fukuda. 2018. Rab7 knockout unveils regulated autolysosome maturation induced by glutamine starvation. *J. Cell Sci.* 131:jcs215442. https://doi.org/10.1242/jcs.215442

Mali, P., L. Yang, K.M. Esvelt, J. Aach, M. Guell, J.E. DiCarlo, J.E. Norville, and G.M. Church. 2013. RNA-guided human genome engineering via Cas9. *Science.* 339:823–826. https://doi.org/10.1126/science.1232033

Martinez, O., A. Schmidt, J. Salaméro, B. Hoflack, M. Roa, and B. Goud. 1994. The small GTP-binding protein rab6 functions in intra-Golgi transport. *J. Cell Biol.* 127:1575–1588. https://doi.org/10.1083/jcb.127.6.1575

Matsui, T., N. Ohbayashi, and M. Fukuda. 2012. The Rab interacting lysosomal protein (RILP) homology domain functions as a novel effector domain for small GTPase Rab36: Rab36 regulates retrograde melanosome transport in melanocytes. *J. Biol. Chem.* 287:28619–28631. https://doi.org/10.1074/jbc.M112.370544

Miserey-Lenkei, S., G. Chalancon, S. Bardin, E. Formstecher, B. Goud, and A. Echard. 2010. Rab and actomyosin-dependent fission of transport vesicles at the Golgi complex. *Nat. Cell Biol.* 12:645–654. https://doi.org/10.1038/ncb2067

Modica, G., O. Skorobogata, E. Sauvageau, A. Vissa, C.M. Yip, P.K. Kim, H. Wurtele, and S. Lefrancois. 2017. Rab7 palmitoylation is required for efficient endosome-to-TGN trafficking. *J. Cell Sci.* 130:2579–2590. https://doi.org/10.1242/jcs.199729

Morita, S., T. Kojima, and T. Kitamura. 2000. Plat-E: an efficient and stable system for transient packaging of retroviruses. *Gene Ther.* 7:1063–1066. https://doi.org/10.1038/sj.gt.3301206

Mrozowska, P.S., and M. Fukuda. 2016. Regulation of podocalyxin trafficking by Rab small GTPases in 2D and 3D epithelial cell cultures. *J. Cell Biol.* 213:355–369. https://doi.org/10.1083/jcb.201512024

Murray, D.H., M. Jahnel, J. Lauer, M.J. Avellaneda, N. Brouilly, A. Cezanne, H. Morales-Navarrete, E.D. Perini, C. Ferguson, A.N. Lupas, et al. 2016. An endosomal tether undergoes an entropic collapse to bring vesicles together. *Nature.* 537:107–111. https://doi.org/10.1038/nature19326

Nachury, M.V., A.V. Loktev, Q. Zhang, C.J. Westlake, J. Peränen, A. Merdes, D.C. Slusarski, R.H. Scheller, J.F. Bazan, V.C. Sheffield, and P.K. Jackson. 2007. A core complex of BBS proteins cooperates with the GTPase Rab8 to promote ciliary membrane biogenesis. *Cell.* 129:1201–1213. https://doi.org/10.1016/j.cell.2007.03.053

Naito, Y., K. Hino, H. Bono, and K. Ui-Tei. 2015. CRISPRdirect: software for designing CRISPR/Cas guide RNA with reduced off-target sites. *Bioinformatics.* 31:1120–1123. https://doi.org/10.1093/bioinformatics/btu743

Opdam, F.J., A. Echard, H.J. Croes, J.A. van den Hurk, R.A. van de Vorstenbosch, L.A. Ginsel, B. Goud, and J.A. Fransen. 2000. The small GTPase Rab6B, a novel Rab6 subfamily member, is cell-type specifically expressed and localised to the Golgi apparatus. *J. Cell Sci.* 113:2725–2735.

Park, S.-Y., J.-S. Yang, A.B. Schmider, R.J. Soberman, and V.W. Hsu. 2015. Coordinated regulation of bidirectional COPI transport at the Golgi by CDC42. *Nature.* 521:529–532. https://doi.org/10.1038/nature14457

Pfeffer, S.R. 2013. Rab GTPase regulation of membrane identity. *Curr. Opin. Cell Biol.* 25:414–419. https://doi.org/10.1016/j.ceb.2013.04.002

Rai, A., A. Oprisko, J. Campos, Y. Fu, T. Friese, A. Itzen, R.S. Goody, E.M. Gazdag, and M.P. Müller. 2016. bMERB domains are bivalent Rab8 family effectors evolved by gene duplication. *eLife.* 5:e18675. https://doi.org/10.7554/eLife.18675

Ran, F.A., P.D. Hsu, J. Wright, V. Agarwala, D.A. Scott, and F. Zhang. 2013. Genome engineering using the CRISPR-Cas9 system. *Nat. Protoc.* 8:2281–2308. https://doi.org/10.1038/nprot.2013.143

Riederer, M.A., T. Soldati, A.D. Shapiro, J. Lin, and S.R. Pfeffer. 1994. Lysosome biogenesis requires Rab9 function and receptor recycling from endosomes to the *trans*-Golgi network. *J. Cell Biol.* 125:573–582. https://doi.org/10.1083/jcb.125.3.573

Rivera, V.M., X. Wang, S. Wardwell, N.L. Courage, A. Volchuk, T. Keenan, D.A. Holt, M. Gilman, L. Orci, F. Cerasoli Jr., et al. 2000. Regulation of protein secretion through controlled aggregation in the endoplasmic reticulum. *Science.* 287:826–830. https://doi.org/10.1126/science.287.5454.826

Rojas, R., T. van Vlijmen, G.A. Mardones, Y. Prabhu, A.L. Rojas, S. Mohammed, A.J.R. Heck, G. Raposo, P. van der Sluijs, and J.S. Bonifacino. 2008. Regulation of retromer recruitment to endosomes by sequential action of Rab5 and Rab7. *J. Cell Biol.* 183:513–526. https://doi.org/10.1083/jcb.200804048

Saitoh, T., M. Nakayama, H. Nakano, H. Yagita, N. Yamamoto, and S. Yamaoka. 2003. TWEAK induces NF-κB2 p100 processing and long lasting NF-κB activation. *J. Biol. Chem.* 278:36005–36012. https://doi.org/10.1074/jbc.M304266200

Sato, K., P. Roboti, A.A. Mironov, and M. Lowe. 2015. Coupling of vesicle tethering and Rab binding is required for in vivo functionality of the golgin GMAP-210. *Mol. Biol. Cell.* 26:537–553. https://doi.org/10.1091/mbc.E14-10-1450

Sato, T., S. Mushiake, Y. Kato, K. Sato, M. Sato, N. Takeda, K. Ozono, K. Miki, Y. Kubo, A. Tsuji, et al. 2007. The Rab8 GTPase regulates apical protein localization in intestinal cells. *Nature.* 448:366–369. https://doi.org/10.1038/nature05929

Sato, T., T. Iwano, M. Kunii, S. Matsuda, R. Mizuguchi, Y. Jung, H. Hagiwara, Y. Yoshihara, M. Yuzaki, R. Harada, and A. Harada. 2014. Rab8a and Rab8b are essential for several apical transport pathways but insufficient for ciliogenesis. *J. Cell Sci.* 127:422–431. https://doi.org/10.1242/jcs.136903

Saucan, L., and G.E. Palade. 1994. Membrane and secretory proteins are transported from the Golgi complex to the sinusoidal plasmalemma of hepatocytes by distinct vesicular carriers. *J. Cell Biol.* 125:733–741. https://doi.org/10.1083/jcb.125.4.733

Seaman, M.N.J. 2004. Cargo-selective endosomal sorting for retrieval to the Golgi requires retromer. *J. Cell Biol.* 165:111–122. https://doi.org/10.1083/jcb.200312034

Shafaq-Zadah, M., C.S. Gomes-Santos, S. Bardin, P. Maiuri, M. Maurin, J. Iranzo, A. Gautreau, C. Lamaze, P. Caswell, B. Goud, and L. Johannes. 2016. Persistent cell migration and adhesion rely on retrograde

transport of β₁ integrin. *Nat. Cell Biol.* 18:54–64. https://doi.org/10.1038/ncb3287

Short, B., C. Preisinger, R. Körner, R. Kopajtich, O. Byron, and F.A. Barr. 2001. A GRASP55-rab2 effector complex linking Golgi structure to membrane traffic. *J. Cell Biol.* 155:877–883. https://doi.org/10.1083/jcb.200108079

Simonsen, A., R. Lippé, S. Christoforidis, J.M. Gaullier, A. Brech, J. Callaghan, B.H. Toh, C. Murphy, M. Zerial, and H. Stenmark. 1998. EEA1 links PI₃K function to Rab5 regulation of endosome fusion. *Nature.* 394:494–498. https://doi.org/10.1038/28879

Sobajima, T., S. Yoshimura, T. Iwano, M. Kunii, M. Watanabe, N. Atik, S. Mushiake, E. Morii, Y. Koyama, E. Miyoshi, and A. Harada. 2014. Rab11a is required for apical protein localisation in the intestine. *Biol. Open.* 4:86–94. https://doi.org/10.1242/bio.20148532

Stenmark, H. 2009. Rab GTPases as coordinators of vesicle traffic. *Nat. Rev. Mol. Cell Biol.* 10:513–525. https://doi.org/10.1038/nrm2728

Storrie, B., M. Micaroni, G.P. Morgan, N. Jones, J.A. Kamykowski, N. Wilkins, T.H. Pan, and B.J. Marsh. 2012. Electron tomography reveals Rab6 is essential to the trafficking of *trans*-Golgi clathrin and COPI-coated vesicles and the maintenance of Golgi cisternal number. *Traffic.* 13:727–744. https://doi.org/10.1111/j.1600-0854.2012.01343.x

Tisdale, E.J., J.R. Bourne, R. Khosravi-Far, C.J. Der, and W.E. Balch. 1992. GTP-binding mutants of rab1 and rab2 are potent inhibitors of vesicular transport from the endoplasmic reticulum to the Golgi complex. *J. Cell Biol.* 119:749–761. https://doi.org/10.1083/jcb.119.4.749

Vogel, G.F., K.M. Klee, A.R. Janecke, T. Müller, M.W. Hess, and L.A. Huber. 2015. Cargo-selective apical exocytosis in epithelial cells is conducted by Myo5B, Slp4a, Vamp7, and Syntaxin 3. *J. Cell Biol.* 211:587–604. https://doi.org/10.1083/jcb.201506112

Wang, T., K. Birsoy, N.W. Hughes, K.M. Krupczak, Y. Post, J.J. Wei, E.S. Lander, and D.M. Sabatini. 2015. Identification and characterization of essential genes in the human genome. *Science.* 350:1096–1101. https://doi.org/10.1126/science.aac7041

Wu, X.S., K. Rao, H. Zhang, F. Wang, J.R. Sellers, L.E. Matesic, N.G. Copeland, N.A. Jenkins, and J.A. Hammer III. 2002. Identification of an organelle receptor for myosin-Va. *Nat. Cell Biol.* 4:271–278. https://doi.org/10.1038/ncb760

Yasuda, T., C. Saegusa, S. Kamakura, H. Sumimoto, and M. Fukuda. 2012. Rab27 effector Slp2-a transports the apical signaling molecule podocalyxin to the apical surface of MDCK II cells and regulates claudin-2 expression. *Mol. Biol. Cell.* 23:3229–3239. https://doi.org/10.1091/mbc.e12-02-0104

Yu, S., G. Yehia, J. Wang, E. Stypulkowski, R. Sakamori, P. Jiang, B. Hernandez-Enriquez, T.S. Tran, E.M. Bonder, W. Guo, et al. 2014. Global ablation of the mouse Rab11a gene impairs early embryogenesis and matrix metalloproteinase secretion. *J. Biol. Chem.* 289:32030–32043.

Yurchenco, P.D. 2011. Basement membranes: cell scaffoldings and signaling platforms. *Cold Spring Harb. Perspect. Biol.* 3:a004911. https://doi.org/10.1101/cshperspect.a004911